Received: 21 August 2017 | Revised: 25 September 2017 | Accepted: 26 September 2017
DOI: 10.1002/aoc.4151

FULL PAPER

WILEY Applied Organometallic Chemistry

Magnetic-based picolinaldehyde–melamine copper complex for the one-pot synthesis of hexahydroquinolines via Hantzsch four-component reactions

Ardeshir Khazaei | Maryam Mahmoudiani Gilan | Negin Sarmasti

Faculty of Chemistry, Bu-Ali Sina University, Hamedan 6517838683, Iran

Correspondence
Ardeshir Khazaei, Faculty of Chemistry, Bu-Ali Sina University, Hamedan 6517838683, Iran.
Email: khazaei_1326@yahoo.com

Funding information
development of chemical methods, reagents and molecules, Grant/Award Number: 32-1716; Center of Excellence in Development of Chemical Method (CEDCM), Hamedan, Iran; Research Affairs Office of Bu-Ali Sina University, Grant/Award Number: 32-1716

A picolinaldehyde–melamine copper complex was loaded on a magnetic Fe_3O_4 core, so that it contained 0.33 mmol of Cu per gram, and was used as an efficient catalyst. The as-synthesized catalyst was characterized using various techniques, including Fourier transform infrared spectroscopy, X-ray diffraction, energy-dispersive X-ray spectroscopy, field emission scanning electron microscopy, transmission electron microscopy, vibrating sample magnetometry and thermogravimetric analysis. The catalyst was used to activate the raw materials in the synthesis of hexahydroquinoline derivatives in one-pot four-component reactions. Low reaction time (minutes versus half an hour), solvent-free condition and magnetically separable catalyst are some salient features of the developed catalyst. Also, the optimum amount of catalyst and temperature were determined as 0.07 g and 87.6 °C, respectively, which were obtained using response surface methodology and optimization techniques.

KEYWORDS
design of experiment, hexahydroquinolines, one-pot reaction, picolinaldehyde–melamine copper complex

1 | INTRODUCTION

Given the number of substances involved in a reaction, reactions in organic chemistry fall into three main categories, namely one-component reactions, two-component reactions and one-pot multicomponent reactions (MCRs).[1] In MCRs, three or more starting materials are involved in the reaction, so that the majority of the atoms of the raw materials are incorporated in the final product.[2] MCRs are also called domino reactions or tandem reactions. The first research in this area is attributed to Gerhard and Laurent who synthesized cyanohydrin imines from bitter almond oil and ammonia,[2] and seminal work was carried out by Strecker (synthesis of α-amino acid from NH_3, aldehyde and HCN).[3] In 1890, Hantzsch synthesized the major constituents of haemoglobin and chlorophyll using MCRs.[2] This was followed by further research, so that now it is a rapidly advancing area, as apparent from several recently published works. Some prototypic examples of MCRs are Mannich three-component reaction (3-CR),[4] Strecker 3-CR,[5,6] Passerini 3-CR,[7,8] Ugi 3-CR,[9] Pauson–Khand 3-CR,[10] Van Leusen 3-CR,[11] Gewald 3-CR,[12] Hantzsch 3-CR[13] and Staudinger 3-CR.[14] In 1881, Hantzsch synthesized dihydropyridine (DHP) which is the one of the most important and conventional MCRs.[13] Due to the diversity and stability of the products, the Hantzsch approach has remained the most widely accepted methodology for the synthesis of DHPs. The various biological properties of DHPs, for instance nifedipine, nicardipine, and amlodipine for the treatment of hypertension,[15,16] have motivated researchers to synthesize novel DHP derivatives which are more effective and with novel modes of action.[17,18] Regarding this issue, Safak's group, by incorporating a fused ring on the DHP structure, synthesized hexahydroquinolines (HHQs) as novel derivatives.[19] The HHQs have widespread pharmacological properties such as vasodilatory, bronchodilatory, anti-atherosclerotic, anti-tumour, geroprotective, hepatoprotective and anti-diabetic activities.[20–22] Analysing the literature shows that the published articles in this area are increasing, with 212 papers hitherto. Synthesis of novel HHQ derivatives via efficient approaches and evaluation of the pharmacological properties are the main aims of the research. Considering the above discussion, various catalysts such as γ-Fe_2O_3,[23] SBA-15/SO_3H nanoreactor,[24] KH_2PO_4,[25] sulfamic acid-functionalized nano-titanium dioxide,[26] nano-$CoAl_2O_4$,[27] nano-ZrO_2-SO_3H,[28] $ZrOCl_2{\cdot}8H_2O$,[29] silica-bonded imidazolium–sulfonic acid chloride,[30] nano-Fe_3O_4–TiO_2–SO_3H,[31] 1,3-disulfonic acid imidazolium hydrogen sulfate,[32] amino alcohol,[33] basic isoreticular metal–organic framework (IRMOF-3),[34] SBA-SO_3H,[35] [MPIm][HSO_4]@SBA-15,[36] SBA-15/$NHSO_3H$[37] and ionic liquids grafted onto graphene oxide[38] have been used in the synthesis of HHQs and DHPs. Although impressive successes have been achieved, most of the developed catalysts suffer from long reaction time (half an hour to several hours), and not so simple procedures for separation of the catalyst. So, there is still a great desire for the synthesis of novel catalysts which are efficient, feasible, high-yielding and with low reaction times.

In the light the above discussion, in the work presented here, we extended the synthetic applicability of an as-prepared catalyst (magnetic-based picolinaldehyde–melamine copper complex) in the synthesis of HHQs in one-pot reactions and under solvent-free condition with low reaction times.

2 | EXPERIMENTAL

2.1 | Materials and apparatus

All chemicals were supplied from Merck and Fluka. The products were characterized using ^1H NMR and ^{13}C NMR spectroscopy, melting points as well as infrared (IR) spectroscopy. The relevant spectral data are given in the supporting information. The ^1H NMR and ^{13}C NMR (500 MHz) spectra were recorded with a Bruker Avance DPX-400 FT-NMR spectrometer (δ in ppm). Melting points were measured using a Büchi B-545 apparatus in open capillary tubes. A PerkinElmer PE-1600-FTIR spectrometer was used to record the IR spectra of products. To measure the mass reduction of the catalyst, thermogravimetric analysis (TGA) under a nitrogen atmosphere was used. Field emission scanning electron microscopy (FESEM) and transmission electron microscopy (TEM) images were recorded with a SIGMA VP-500 (Zeiss) and Zeiss-EM10C-100 KV, respectively. Elemental analysis of the as-synthesized catalyst was conducted using energy-dispersive X-ray analysis (EDX; Oxford Instruments). A vibrating sample magnetometer (model MDKB) was used to determine the saturation magnetization of the catalyst. To monitor reaction progress, TLC (using silica gel SIL G/UV 254 plates) was used.

2.2 | Synthesis of catalyst

2.2.1 | Synthesis of Fe_3O_4 nanoparticles

Magnetic Fe_3O_4 nanoparticles were synthesized using the co-precipitation method.[39] First, 11.3 g of $FeCl_3{\cdot}6H_2O$ and 5.6 g of $FeCl_2{\cdot}4H_2O$ were dissolved in deionized water at 80 °C with mixing (600 rpm). After complete dissolution of the salts, 25 ml of ammonia (28 wt%) was added rapidly to the solution.[40] The resulting black solution was vigorously stirred for 2 h at 80 °C under nitrogen atmosphere. Then the precipitated magnetic nanoparticles were separated from the solution using a magnet. They were washed several times with water and then with acetone. Finally a stable black magnetic dispersion was obtained and dried in an oven.

2.2.2 | Synthesis of magnetic Fe_3O_4@SiO_2 nanoparticles

An amount of 1 g of the Fe_3O_4 nanoparticles was dispersed in water and ethanol mixture (80:20 v/v) using an ultrasound bath (15 min). Then 2 ml of ammonia (28 wt%) and 2 ml of tetramethyl orthosilicate were added dropwise to the mixture and stirred at 50 °C for 2 h. The obtained Fe_3O_4@SiO_2 nanoparticles were separated using a magnet and then washed with water and ethanol successively, and dried in an oven.

2.2.3 | Synthesis of Fe_3O_4@SiO_2@Si-$(CH_2)_3Cl$ nanoparticles

An amount of 1 g of the previously synthesized Fe_3O_4@SiO_2 nanoparticles was dispersed in 50 ml of toluene (15 min). Then 2 ml of (3-chloropropyl) triethoxysilane was gently added to the mixture and refluxed at 110 °C for 24 h. The synthesized nanoparticles were separated using a magnet and washed several times with toluene and water. Finally the product was dried in an oven.

2.2.4 | Synthesis of $Fe_3O_4@SiO_2@Si$-$(CH_2)_3$@melamine nanoparticles

Amounts of 12 mmol (1.51 g) of melamine and 12 mmol of K_2CO_3 as a base were dissolved in 70 ml of dimethylsulfoxide (DMSO), and then 1 g of the $Fe_3O_4@SiO_2@Si$-$(CH_2)_3Cl$ nanoparticles was added to the mixture and dispersed (15 min). After refluxing the mixture for 24 h, the nanoparticles were separated using magnet, washed with 50 ml of DMSO and dried in an oven.

2.2.5 | Synthesis of $Fe_3O_4@SiO_2@Si$-$(CH_2)_3$@melamine@picolinaldehyde nanoparticles

First, 1 g of the $Fe_3O_4@SiO_2@Si$-$(CH_2)_3$@melamine nanoparticles was dispersed in 50 ml of methanol (15 min), and refluxed. An amount of 24 mmol of picolinaldehyde (2.57 g) was dissolved in 30 ml of methanol, and then was added dropwise to the nanoparticles using a decanter funnel. After refluxing for 24 h, the product was separated using a magnet, washed with 50 ml of methanol and dried in an oven.

2.2.6 | Synthesis of $Fe_3O_4@SiO_2@Si$-$(CH_2)_3$@melamine@picolinaldehyde@Cu nanoparticles

A solution of $Cu(OAc)_2$ (5% w/v) was prepared in methanol (solution A), and then 1 g of the nanoparticles synthesized in the previous step was dispersed in 50 ml of methanol (15 min). Solution A was added dropwise to the dispersed nanoparticles, and the resulting mixture refluxed for 48 h. After the completion of the reaction, the nanoparticles were separated using a super magnet, and washed several times with methanol. The final product was dried in an oven. The overall scheme for the synthesis of the nanoparticles and catalyst is shown in Figure 1.

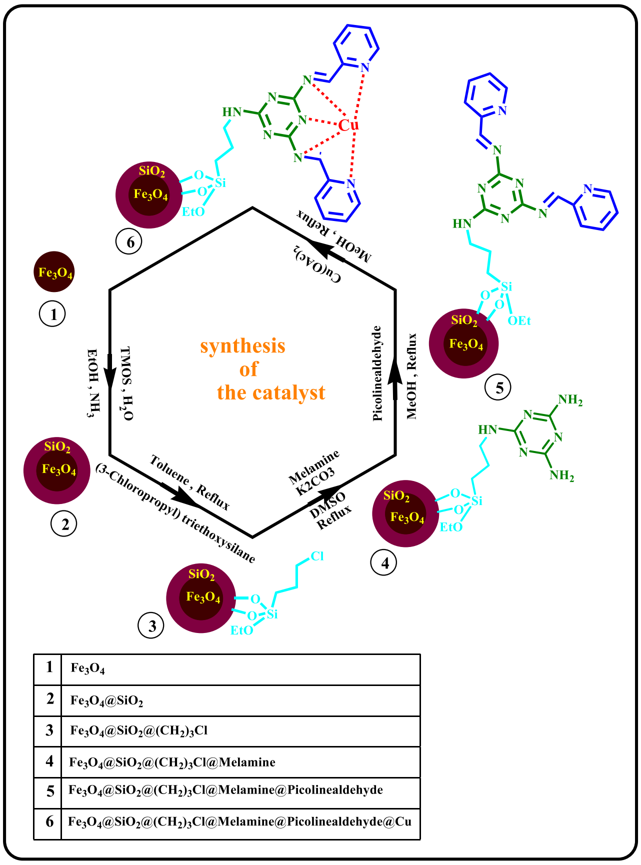

1	Fe_3O_4
2	$Fe_3O_4@SiO_2$
3	$Fe_3O_4@SiO_2@(CH_2)_3Cl$
4	$Fe_3O_4@SiO_2@(CH_2)_3Cl$@Melamine
5	$Fe_3O_4@SiO_2@(CH_2)_3Cl$@Melamine@Picolinealdehyde
6	$Fe_3O_4@SiO_2@(CH_2)_3Cl$@Melamine@Picolinealdehyde@Cu

FIGURE 1 Total procedure for synthesis of catalyst

2.3 | General procedure for synthesis of HHQs

Using the optimum benchmark reaction conditions, namely 0.06 g of as-prepared catalyst and at 50 °C, dimedone (0.28 g, 2 mmol), aryl aldehyde (2 mmol), β-ketoester (2 mmol) and ammonium acetate (0.185 g, 2.4 mmol) were added to a test tube, and then the mixture was stirred magnetically. TLC was used to probe the reaction progress, and after completion of the reaction, the mixture was cooled to room temperature. Then, 20 ml of hot ethyl acetate was added to the reaction mixture, so that all of the components were dissolved, and because of the insolubility of the catalyst, it was recovered with a super magnet. Finally the product was purified by crystallization from the added ethyl acetate.

2.4 | Retrieval of catalyst

To investigate the catalytic activity versus the number of reaction cycles, the benchmark reaction was carried out. After the complete progress of the reaction, 20 ml of hot ethyl acetate was added to the reaction mixture to dissolve all the raw material and final product. To cancel out the reaction time, all of the cycles were ended after 6 min. Then, the catalyst was separated with a super magnet. The resulting solution without any work-up was used for crystallization of the product. The catalyst was dried in an oven and utilized in the next cycle. Figure 2 shows the reaction yield versus number of cycles. As can be seen, the reaction yield does not change significantly, which implies that the catalytic activity remains almost unchanged. It should be noted that all reaction cycles were performed at optimum conditions.

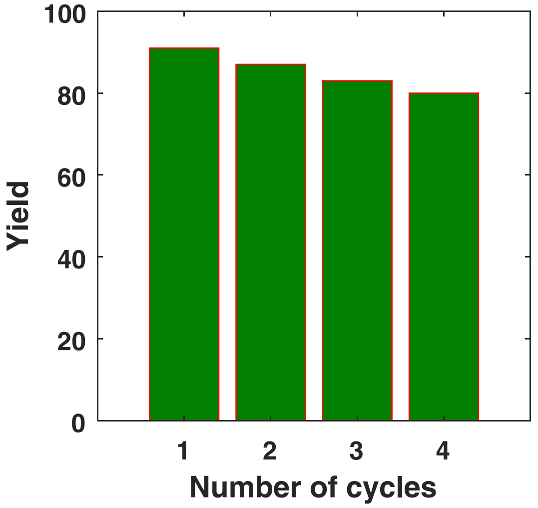

FIGURE 2 Benchmark reaction yield versus number of cycles

3 | RESULTS AND DISCUSSION

3.1 | Characterization of catalyst

The IR spectra of the intermediate nanoparticles and final catalyst are shown in Figure 3. The band at 1083.24 cm^{-1} belongs to SiO of the SiO_2 group in the $Fe_3O_4@SiO_2$ nanoparticles, and that at 2946.4 cm^{-1} is related to CH_2 of propyl chloride in $Fe_3O_4@SiO_2@Si(CH_2)_3Cl$ nanoparticles. The band at 3282.3 cm^{-1} is an indication of the presence of NH_2 group of melamine, confirming the loading of melamine on the surface of $Fe_3O_4@SiO_2@Si(CH_2)_3Cl$. It has been shown that melamine with three nitrogen atoms can well coordinate with metal ions such as copper.[41–43] The band at 1428 cm^{-1} corresponds to the CH_3COO^- group, and that at 497 cm^{-1} is attributed to O—Cu[41] and C=N. The band at 1568 cm^{-1} can arise from the complexation of copper ions to the imine group and then it shifts from 1699 to 1568 cm^{-1}. These bands imply the formation of the complex between picolinaldehyde, melamine and copper.

Vibrating sample magnetometry was used to further verify the loading of various layers on the nanoparticles. The saturation magnetization curves of Fe_3O_4, $Fe_3O_4@SiO_2$ and $Fe_3O_4@SiO_2@Si(CH_2)_3@melamine@picolinaldehyde@Cu$ nanoparticles are shown in Figure 4. As one can see, the saturation magnetization decreases (54, 50 and 43 emu g^{-1} for Fe_3O_4, $Fe_3O_4@SiO_2$ and as-prepared catalyst, respectively) with an increasing number of loaded layers on nano-Fe_3O_4. It has been shown that non-magnetic materials reduce the saturation magnetization because of the quenching of surface moments,[44] and this behaviour is seen clearly in Figure 4. It should be noted that, although the magnetization of the as-prepared catalyst is reduced, it is enough

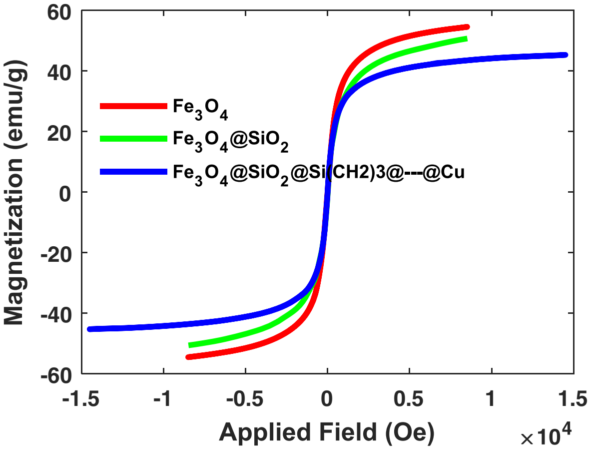

FIGURE 4 Saturation magnetization curves for Fe_3O_4, $Fe_3O_4@SiO_2$ and $Fe_3O_4@SiO_2@Si(CH_2)_3@melamine@picolinaldehyde@Cu$.

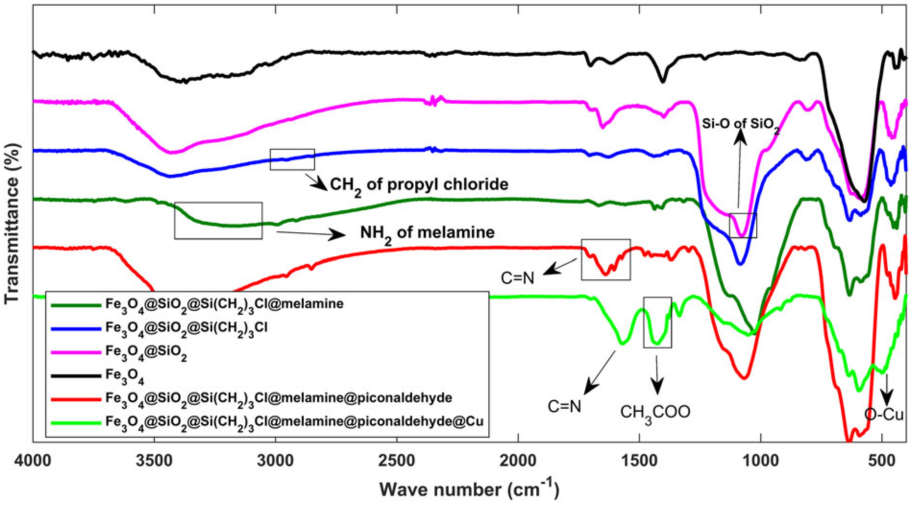

FIGURE 3 IR spectra of intermediate nanoparticles and as-prepared catalyst ($Fe_3O_4@SiO_2@Si\text{-}(CH_2)_3@melamine@picolinaldehyde@Cu$)

such that it can be easily retrieved from the reaction mixture.

FESEM and TEM images of the as-prepared nanomagnetic catalyst are shown in Figure 5. These techniques were used to identify the size, shape and morphology of micro- and nanoparticles. As can be seen from the FESEM images (Figure 5a,b), the geometric shape of the nanoparticles is spherical. Besides the spherical shape, the TEM images (Figure 5c,d) show the catalyst has a core–shell structure. The shell is attributed to the various layers loaded on the Fe_3O_4 surface. Figure 6 shows the normal probability and cumulative particle size distribution (experimental and fitted) of the as-prepared catalyst. The experimentally determined curve in the normal probability plot (Figure 6a) is fairly straight, so the normality of the particle sizes could be a reasonable assumption. The cumulative distribution function (Figure 6b) shows that 60 and 90% of the nanoparticles have sizes of 30 and 40 nm, respectively. The data collected from FESEM images show that the mean and the standard deviation of sizes of as-synthesized catalyst nanoparticles are 29.45 and 7.25 nm, respectively.

The size, purity and crystalline nature of the particles can be identified with the X-ray diffraction (XRD) technique. The XRD patterns of Fe_3O_4, $Fe_3O_4@SiO_2$, $Fe_3O_4@SiO_2@Si(CH_2)_3Cl$ and $Fe_3O_4@SiO_2@Si(CH_2)_3$@melamine@picolinaldehyde@Cu nanoparticles are shown in Figure 7. To calculate the as-synthesized catalyst particle size, the Scherrer equation ($D = K\lambda/\beta\cos\theta$) was used, where K, λ, β and θ correspond to dimensionless shape factor, X-ray wavelength, full width at half maximum (FWHM) of the diffraction peak and Bragg diffraction angle in radians, respectively. It was supposed that the nanoparticles have a spherical geometric shape, so that the K value is set to 0.9 in the Scherrer equation. For the X-ray wavelength (λ), 0.154184 nm was used which is the averaged value ($K\alpha_1$ $\lambda = 0.1540598$ nm and $K\alpha_2$ $\lambda = 0.154433$ nm) of copper $K\alpha$. The values of β and θ are determined from XRD patterns. The values of θ, FWHM and calculated particle size are given in Table 1. Using the Scherrer equation, 9.86 nm was obtained as the mean value of particle size. There is a discrepancy between the mean particle size from FESEM (29.45 nm) and XRD (9.86 nm) techniques. This difference is attributed to the inability to measure small particles in FESEM and the K value in the Scherrer equation.

In addition, the Bragg equation ($d_{hkl} = \lambda/2\sin\theta$) was used to identify the distance between the layers (d-spacing or interplaner spacing) in the crystalline structure of as-prepared catalyst. The d-spacing values at different diffraction angles are given in Table 1.

The EDX technique was used to determine the contribution of each element of the sample. The elemental

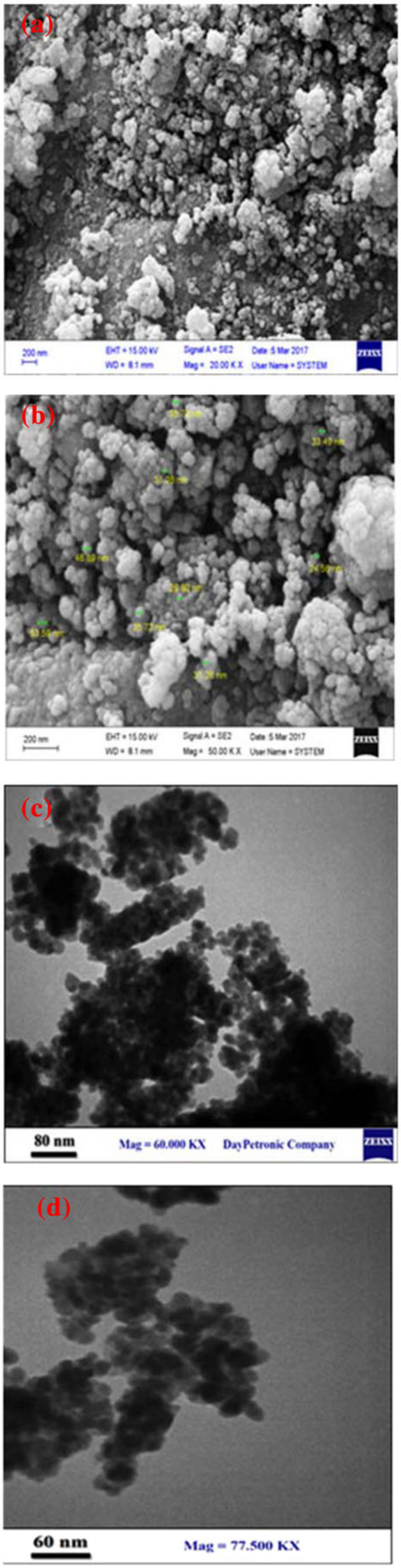

FIGURE 5 (a, b) FESEM and (c, d) TEM images of as-synthesized catalyst

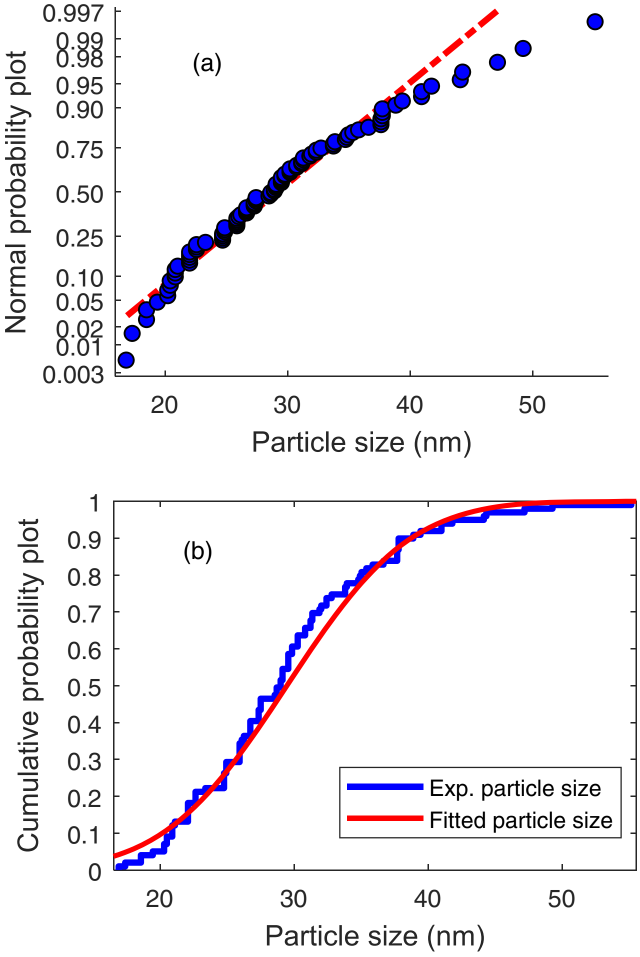

FIGURE 6 (a) Normal probability plot and (b) cumulative probability plot of as-synthesized nanoparticle size

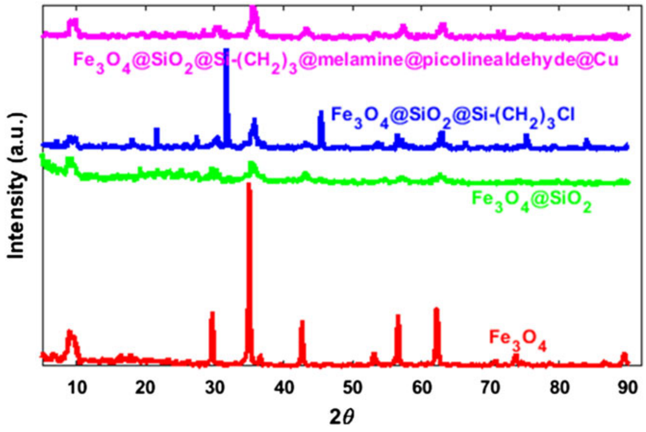

FIGURE 7 XRD patterns of intermediate nanoparticles and as-prepared catalyst ($Fe_3O_4@SiO_2@Si-(CH_2)_3@melamine@picolinaldehyde@Cu$)

analysis of the as-synthesized catalyst together with the contribution of each element is shown in Figure 8. The mass percentages of Fe, O, C, Si, N and Cu are 46.7, 24.6, 17.7, 5.4, 3.5 and 2.1%, respectively. The contribution of Cu shows that 0.33 mmol of Cu per gram of catalyst (0.33 mmol g^{-1}) has been coordinated with the melamine and picolinaldehyde. The Au peak in Figure 8 is due to the coating of the sample with Au in the procedure of sample preparation. There are 5 mmol of N per gram of catalyst, which is approximately 15 times that of Cu. So it can be inferred that half (52.8%) of the picolinaldehyde and melamine have been coordinated with Cu.

The thermal stability of the catalyst has a great effect on its catalytic activity, because the optimum reaction temperature is approximately 88 °C. The TGA curve of the as-prepared catalyst is shown in Figure 9. The first mass loss up to 150 °C (region A) is due to the release of adsorbed water; the second from 200 to 550 °C is related to the decomposition of organic matter on the $Fe_3O_4@SiO_2$ core (region B). Region C corresponds to $Fe_3O_4@SiO_2$. The TGA curve of the catalyst system demonstrates high thermal stability, with decomposition starting at around 200 °C under a nitrogen atmosphere.

3.2 | Effect of solvent on reaction

To determine the effect of solvent type on the reaction yield and time, the benchmark reaction (reaction of benzaldehyde, dimedone, ethyl acetoacetate and ammonium acetate) was carried out (under the optimized reaction conditions) in various solvents, namely ethyl acetate, dimethylformamide (DMF), water, *n*-hexane and ethanol, and under solvent-free condition. Results are given in Table 2. The reaction under solvent-free condition, with 12 min and 85% for reaction time and yield, respectively, is more efficient than reaction with solvent. This can be attributed to the presence of ethyl acetoacetate, which is liquid at room temperature and in the reaction, so that it can play the role of solvent.

3.3 | Experimental design

The yield and time of an organic reaction are affected by numerous factors such as temperature, type and amount of catalyst, type of solvent, and so on. Because of complex interactions between factors, the effect of the different factors cannot be modelled using rigorous mathematical relations. In this situation, statistics can be useful, so that one can perturb the effective variable to measure the response. The conventional method which is used by many chemists is 'change one variable at a time' (OVAT) or interchangeably 'one factor at a time'. If the is a considerable interaction between parameters the OVAT procedure is not efficient, so that it gives an unrealistic optimal point.[29,45,46] The large number of experiments is another relevant feature of this method, so it is not

TABLE 1 XRD data for as-synthesized catalyst (Fe_3O_4@SiO_2@$Si(CH_2)_3$@melamine@picolinaldehyde@Cu)

Entry	2θ (°)	Peak width, FWHM (rad)	Size (nm)	Interplanar spacing of crystal (nm)
1	9.2	1.111	7.16	0.96
2	30.3	0.789	10.8	0.29
3	35.7	0.732	10.9	0.25
4	43.5	0.657	12.1	0.21
5	57.3	0.852	9.33	0.16
6	63.0	0.825	9.64	0.15
Mean	—	—	9.86	0.34

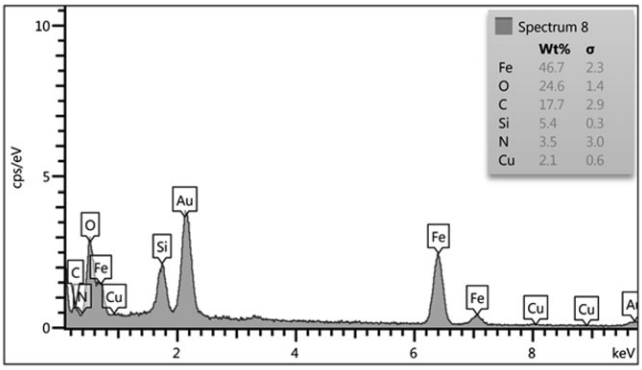

FIGURE 8 Elemental analysis of as-prepared catalyst (Fe_3O_4@SiO_2@$Si(CH_2)_3$@melamine@picolinaldehyde@Cu) using EDX

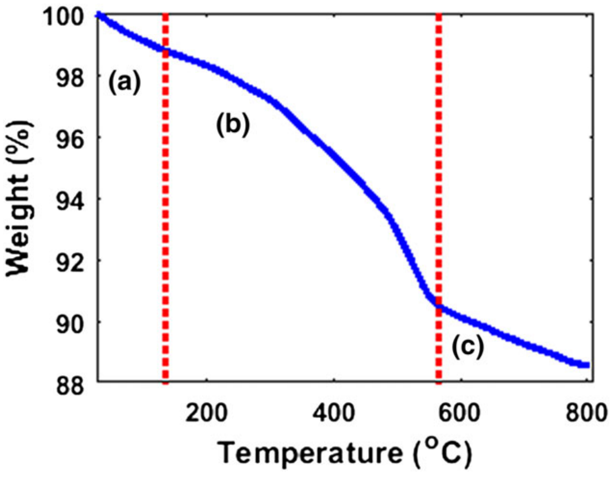

FIGURE 9 TGA curve of as-prepared catalyst (Fe_3O_4@SiO_2@$Si(CH_2)_3$@melamine@picolinaldehyde@Cu)

TABLE 2 Effect of solvents, and no solvent, on the reaction time and yield

Entry	Solvent	Time (min)	Yield at 60° (%)[a]
1	—	12	85
2	EtOAc	>100	52
3	DMF	>100	55
4	H_2O	>100	43
5	*n*-Hexane	>100	35
6	EtOH	90	50

[a] Isolated yield.

efficient from material, time and economic points of view.[47,48] Unfortunately, many researchers probes their optimal conditions through OVAT methodology. Recently, multivariate statistical approaches, namely design of experiment, have been used to overcome the drawbacks of the OVAT method. Although various approaches are used in the design of experiment methodology, the response surface method (RSM) is the most used one. The most well-known RSM is central composite design which is used in the present work to find the optimal conditions in the synthesis of HHQs.

Briefly, the amount of catalyst (X_1) and temperature (X_2) were considered as the effective variables on the reaction yield (Y) at a specified reaction time. The factors X_1 and X_2 were coded to three levels (−1, 0, 1) in face-centred composite design. Three replicates at centre point were used to probe the curvature in response (yield, Y), if there is one. The levels of the variables are given in Table 3. The benchmark reaction (reaction of benzaldehyde, dimedone, ethyl acetoacetate and ammonium acetate) was carried out in these designed experimental runs, with the reaction being stopped after 4 min to cancel out the effect of time on the reaction yield. The reaction yields are given in Table 3. It should be noted that the given yields ate the crystallization yields in ethyl acetate up to ambient temperature as the minimum temperature.

3.4 | Optimization of reaction conditions and validation of model

From a mathematical point of view, the relation between effective variables and dependent variable (response) can be expressed using a Taylor expansion series.[49] In the present work, a second-order Taylor expansion series

TABLE 3 Levels of effective variables and corresponding response values (yield) using face-centred composite design method

Run	Effective variable				Response (yield)
	X_1 (amount of catalyst)		X_2 (temperature)		
	Coded level	Actual level	Coded level	Actual level	
1	0	0.0355	−1	30.00	50
2	0	0.0355	+1	110.00	70
3	−1	0.0010	−1	30.00	38
4	−1	0.0010	+1	110.00	57
5	+1	0.0700	0	70.00	85
6	+1	0.0700	+1	110.00	83
7	0	0.0355	0	70.00	71
8	0	0.0355	0	70.00	72
9	0	0.0355	0	70.00	71
10	−1	0.0010	0	70.00	56
11	+1	0.0700	−1	30.00	65

was used:

$$Y = \beta_0 + \beta_1 x_1 + \beta_2 x_2 + \beta_{12} x_1 x_2 + \beta_{11} x_1^2 + \beta_{22} x_2^2 + \varepsilon \quad (1)$$

where $\beta_0,\ldots,\beta_{22}$ stand for the coefficients of the model and x and Y explain the effective variables and response. The matrix notation of the model is given as:

$$Y = \beta X + \varepsilon \quad (2)$$

To find the best value of the coefficient, the method of least squares was used:[50]

$$\beta = \left(X^{\mathrm{T}} X\right)^{-1} X^{\mathrm{T}} Y \quad (3)$$

The final polynomial model for the reaction yield based on the experimental runs and method of least squares is as follows:

$$Y = 7.70 + 408.82 X_1 + 1.16 X_2 - 0.18 X_1 X_2 - 6.56 \times 10^{-3} X_2^2 \quad (4)$$

Analysis of variance (ANOVA) showed that based on the sum of squares and lack of fit, the quadratic model could well correlate with the experimental data. The summary of ANOVA is given in Table 4, so that the probability value (p-value) is less than 0.0001, which calls for the rejection of the null hypothesis. Although the p-value of the model parameters shows that the X_1X_2 and X_1^2 terms should be cancelled out from equation 4, the model is significant and can be used for further analysis. Although the value of R^2 (0.9974) shows that the provided model could well correlate the experimental reaction yields, the predictive power of the model must be evaluated, which is given as predicted R^2 in Table 4. The value of 0.9787 shows that the model could well predict the reaction yield, with new values of X_1 and X_2 which are not present in Table 3 (temperature and the amount of catalyst which didn't used in the model development procedure).

TABLE 4 Analysis of variance (ANOVA) based on quadratic polynomial model for yield of reaction

Source	Probability value (p-value)
Model (yield)	<0.0001
X_1	<0.0001
X_2	<0.0001
X_1X_2	0.6410
X_1^2	1.0000
X_2^2	<0.0001
R^2	0.9974
Predicted R^2	0.9787
Lack of fit	0.1901

Figure 10 shows graphically the power of the model in correlation and prediction of the reaction yield. Any deviation from the diagonal line indicates the inability of model to correlate or predict the experimental data or the error of the experimental yield data.

Figure 11 shows the three-dimensional surface and the contours of reaction yield versus amount of catalyst and temperature. As one can see, an increased yield, Y, is achieved through an increase in the amount of catalyst, X_1, with a positive value of β_1 in equation 4. As the temperature increases, the reaction yield first increases to a maximum value, and then decreases. An increase in the yield is likely to be attributed to the temperature dependence of the reaction kinetics,

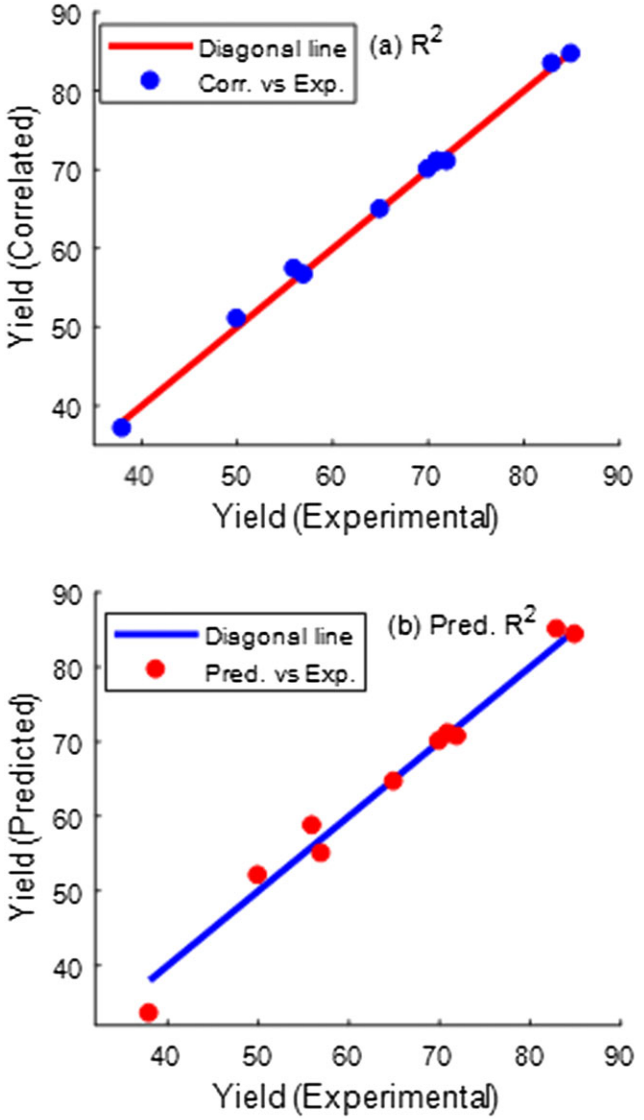

FIGURE 10 R^2 and predicted R^2 of reaction yield from the obtained model

and a decrease of the yield is probably related to the loss of catalytic activity at higher temperatures.

To determine the optimum point (using analytical or numerical methods) of the yield, equation 4 was used, with 0.07 g and 87.6 °C being obtained for the amount of catalyst and temperature, respectively. Although the predictive power of the model was evaluated using predicted R^2, it is better evaluate the model at a new point. So, the yield of the optimum point was obtained in the laboratory and compared with the results of the model, which are given in Table 5. The deviation between the experimental and predicted yield is 4.46%, which is low enough for a predictive model. Accordingly, the obtained results are compared with those of experimental and a good agreement between them is noticed.

To further investigate the effect of catalyst on reaction time, the obtained optimum point was repeated in the laboratory without catalyst. The results are given in Table 6. As one can see, in the absence of catalyst, even with a time greater than 30 min, the yield is low (56%). So, the

TABLE 5 Predicted and experimental values of reaction yield at optimum point

	Optimum variable		Optimum response	
	X_1	X_2	Time (min)	Yield (%)
Predicted	0.07	87.6	4	86.7
Experimental	0.07	88.0	4	83.0

TABLE 6 Checking optimum condition with and without catalyst

	Variable		Response	
Condition	X_1	X_2	Time (min)	Yield (%)
With catalyst	0.07	88.0	6	91.0
Without catalyst	—	88.0	>30	56.0

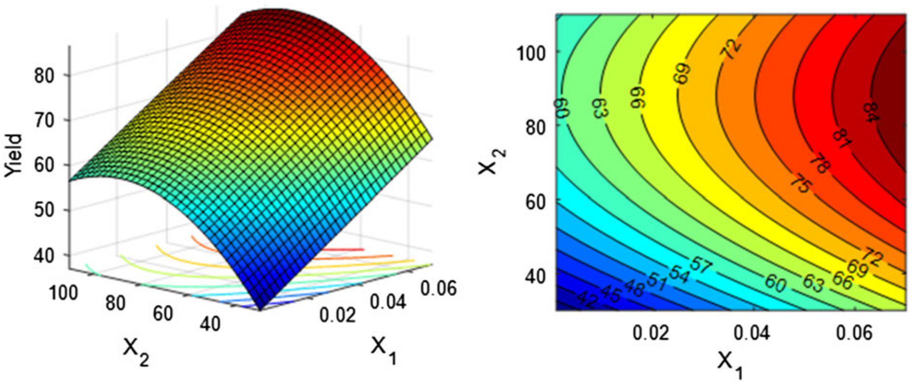

FIGURE 11 Surface and contour of reaction yield versus amount of catalyst and temperature

TABLE 7 HHQ derivatives synthesized under optimum conditions

Product	1	2	3	4	5	6
	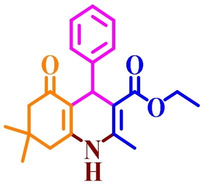	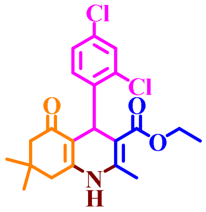	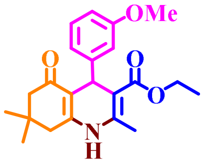	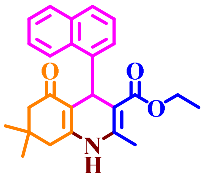	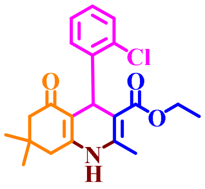	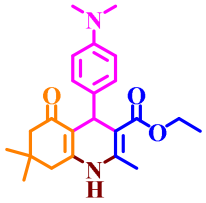
M.p. (°C)	218–221	242–244	203–205	205–206	200–204	234–236
Yield (%)	91	71	79	84	93	92
Time (min)	6	5	10	5	6	37
Ref.	[51]	[33]	[29]	[52]	[53]	[29]
Product	7	8	9	10	11	12
	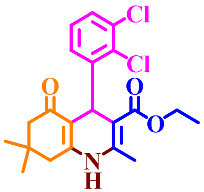	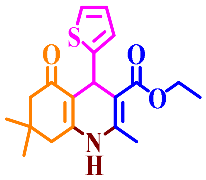	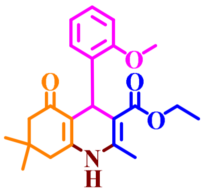	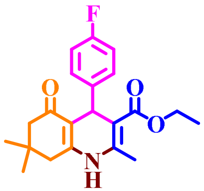	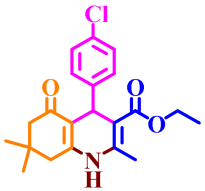	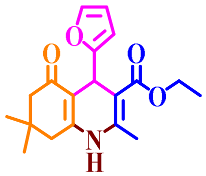
M.p. (°C)	229–231	243–245	255–256	186–189	240–242	246–249
Yield (%)	82	77	88	71	81	75
Time (min)	2	9	8	17	4	17
Ref.	[29]	[53]	[29]	[53]	[53]	[53]

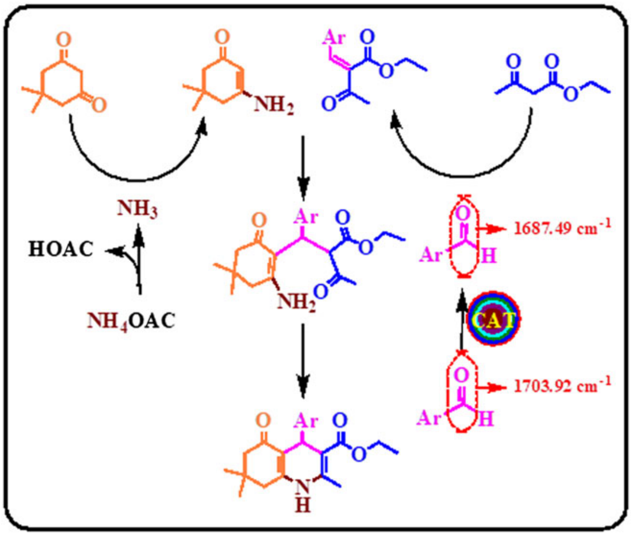

FIGURE 12 Plausible mechanism for synthesis of HHQ using as-synthesized catalyst

presence of the catalyst is vital for the progress of the reaction.

3.5 | Synthesis of HHQs at optimal conditions

Although the optimum point was achieved through the benchmark reaction, it was assumed that the optimum point is fixed for all the benzaldehyde derivatives. Hence, reactions between various aryl aldehydes, dimedone, ethyl acetoacetate and ammonium acetate were carried out at the optimum condition ($X_1 = 0.07$ g and $X_2 = 87$ °C). Various aryl aldehyde derivatives with electron-withdrawing and electron-donating groups on the benzene ring were successfully examined. The products of the reactions together with the experimental melting points are given in Table 7. Although the reaction yields are almost identical to those reported in the literature, for some derivatives such as products **1**, **9** and **11**,[26,32,33,51–53] the reaction time is short (minutes versus half an hour) and for some products, including **3**, **6** and **12**, the reaction time is longer than those reported.[52,53]

3.6 | Proposed mechanism

A proposed and plausible mechanism based on IR data is shown in Figure 12. As shown, and based on IR investigations, the as-prepared catalyst interacts only with benzaldehyde and reduces the carbonyl band wavenumber from 1703.92 to 1687.49 cm^{-1}. The details of the mechanism, along with the associated intermediates, are presented in the literature.[29,54]

4 | CONCLUSIONS

In summary, a magnetic-based picolinaldehyde–melamine copper complex was synthesized and used in the synthesis of HHQ derivatives. The synthesized catalyst contains 0.33 mmol of Cu per gram which can activate the reaction between starting materials. The as-synthesized catalyst has salient features which include: magnetically separation of the catalyst, solvent-free condition, green, benign and considerable short reaction time. Face-centred composite design as a response surface methodology was used to statistically design the experimental runs. Using the obtained quadratic polynomial model for the reaction yield, and with the optimization techniques, the true maximum was achieved. So, the RSM method in this case is more efficient than OVAT.

ACKNOWLEDGEMENTS

The authors gratefully acknowledge partial support of this work by the Research Affairs Office of Bu-Ali Sina University (grant number 32-1716, entitled development of chemical methods, reagents and molecules), Center of Excellence in Development of Chemical Method (CEDCM), Hamedan, Iran.

ORCID

Ardeshir Khazaei http://orcid.org/0000-0001-7990-2266

REFERENCES

[1] T. Zarganes-Tzitzikas, A. L. Chandgude, A. Dömling, *Chem. Rec.* **2015**, *15*, 981.

[2] I. Ugi, A. Dömling, W. Hörl, *Endeavour* **1994**, *18*, 115.

[3] Z. Wang, *Strecker Synthesis: Comprehensive Organic Name Reactions and Reagents*, John Wiley, New York **2010**.

[4] C. Mannich, W. Krösche, *Arch. Pharm.* **1912**, *250*, 647.

[5] A. Strecker, *Justus Liebigs Ann. Chem.* **1850**, *75*, 27.

[6] J. T. Kuethe, D. R. Gauthier, G. L. Beutner, N. Yasuda, *J. Org. Chem.* **2007**, *72*, 7469.

[7] M. Passerini, L. Simone, *Gazz. Chim. Ital.* **1921**, *51*, 126.

[8] S. Rostamnia, *RSC Adv.* **2015**, *5*, 97044.

[9] I. Ugi, *Angew. Chem. Int. Ed. Engl.* **1962**, *1*, 8.

[10] P. L. Pauson, I. U. Khand, *Ann. N. Y. Acad. Sci.* **1977**, *295*, 2.

[11] A. M. Van Leusen, J. Wildeman, O. H. Oldenziel, *J. Org. Chem.* **1977**, *42*, 1153.

[12] K. Gewald, E. Schinke, H. Böttcher, *Chem. Ber.* **1966**, *99*, 94.

[13] A. Hantzsch, *Ber. Deutsch. Chem. Gesellsch.* **1881**, *14*, 1637.

[14] H. Staudinger, *Justus Liebigs Ann. Chem.* **1907**, *356*, 51.

[15] N. Edraki, A. R. Mehdipour, M. Khoshneviszadeh, R. Miri, *Drug Discov. Today* **2009**, *14*, 1058.

[16] J. L. Reid, P. A. Meredith, F. Pasanisi, *J. Cardiovasc. Pharmacol.* **1985**, *7*, S18.

[17] D. Längle, V. Marquardt, E. Heider, B. Vigante, G. Duburs, I. Luntena, D. Flötgen, C. Golz, C. Strohmann, O. Koch, D. Schade, *Eur. J. Med. Chem.* **2015**, *95*, 249.

[18] J. Marín-Prida, G. L. Pardo Andreu, C. P. Rossignoli, M. G. Durruthy, E. O. Rodríguez, Y. V. Reyes, R. F. Acosta, S. A. Uyemura, L. C. Alberici, *Toxicol. In Vitro* **2017**, *42*(Suppl. C), 21.

[19] C. Safak, R. Simsek, *Mini-Rev. Med. Chem.* **2006**, *6*, 747.

[20] T. Godfraind, R. Miller, M. Wibo, *Pharmacol. Rev.* **1986**, *38*, 321.

[21] R. Mannhold, B. Jablonka, W. Voigt, K. Schönafinger, E. Schraven, *Eur. J. Med. Chem.* **1992**, *27*, 229.

[22] E. Baydar, M. G. Gündüz, V. S. Krishna, R. Şimşek, D. Sriram, S. Ö. Yıldırım, R. J. Butcher, C. Şafak, *Res. Chem. Intermed.* **2017**, https://doi.org/10.1007/s11164-017-3087-0.

[23] S. Rostamnia, A. Nuri, H. Xin, A. Pourjavadi, S. H. Hosseini, *Tetrahedron Lett.* **2013**, *54*, 3344.

[24] S. Rostamnia, H. Xin, X. Liu, K. Lamei, *J. Mol. Catal. A* **2013**, *374*(Suppl. C), 85.

[25] S. J. Yü, S. Wu, X. M. Zhao, C. W. Lü, *Res. Chem. Intermed.* **2017**, *43*, 3121.

[26] E. Tabrizian, A. Amoozadeh, *J. Chinese Chem. Soc.* **2017**, *64*, 331.

[27] A. Khazaei, L. Jafari-Ghalebabakhani, E. Ghaderi, M. Tavasoli, A. R. Moosavi-Zare, *Appl. Organometal. Chem.* **2017**, https://doi.org/10.1002/aoc.3815.

[28] A. Amoozadeh, S. Rahmani, M. Bitaraf, F. B. Abadi, E. Tabrizian, *New J. Chem.* **2016**, *40*, 770.

[29] A. Khazaei, N. Sarmasti, J. Y. Seyf, M. Tavasoli, *RSC Adv.* **2015**, *5*, 101268.

[30] A. R. Moosavi-Zare, M. A. Zolfigol, M. Zarei, A. Zare, J. Afsar, *Appl. Catal. A* **2015**, *505*, 224.

[31] A. Amoozadeh, S. Golian, S. Rahmani, *RSC Adv.* **2015**, *5*, 45974.

[32] A. Zare, F. Abi, A. R. Moosavi-Zare, M. H. Beyzavi, M. A. Zolfigol, *J. Mol. Liq.* **2013**, *178*, 113.

[33] S.-J. Song, Z.-X. Shan, Y. Jin, *Synth. Commun.* **2010**, *40*, 3067.

[34] S. Rostamnia, H. Xin, *Appl. Organometal. Chem.* **2014**, *28*, 359.

[35] E. Doustkhah, S. Rostamnia, A. Hassankhani, *J. Porous Mater.* **2016**, *23*, 549.

[36] S. Rostamnia, A. Hassankhani, H. G. Hossieni, B. Gholipour, H. Xin, *J. Mol. Catal. A* **2014**, *395*(Suppl. C), 463.

[37] S. Rostamnia, A. Hassankhani, *Synlett* **2014**, *25*, 2753.

[38] S. Sobhani, F. Zarifi, J. Skibsted, *New J. Chem.* **2017**, *41*, 6219.

[39] X. Liu, Z. Ma, J. Xing, H. Liu, *J. Magn. Magn. Mater.* **2004**, *270*, 1.

[40] S. Rostamnia, B. Zeynizadeh, E. Doustkhah, A. Baghban, K. O. Aghbash, *Catal. Commun.* **2015**, *68*, 77.

[41] Y.-P. Wang, Y. Luo, R.-M. Wang, *React. Funct. Polym.* **1997**, *33*, 81.

[42] A. B. Wiles, D. Bozzuto, C. L. Cahill, R. D. Pike, *Polyhedron* **2006**, *25*, 776.

[43] D. M. L. Goodgame, I. Hussain, A. J. P. White, D. J. Williams, *J. Chem. Soc. Dalton Trans.* **1999**, *16*, 2899.

[44] H. Xu, N. Tong, L. Cui, Y. Lu, H. Gu, *J. Magn. Magn. Mater.* **2007**, *311*, 125.

[45] M. A. Zolfigol, A. Khazaei, N. Sarmasti, J. Y. Seyf, V. Khakyzadeh, A. R. Moosavi-Zare, *J. Mol. Catal. A* **2014**, *393*, 142.

[46] D. D. Frey, F. Engelhardt, E. M. Greitzer, *Res. Eng. Des.* **2003**, *14*, 65.

[47] R. Carlson, J. E. Carlson, *Design and Optimization in Organic Synthesis*, Elsevier Science, Oxford **2005**.

[48] F. Paulo, L. Santos, *Mater. Sci. Eng. C* **2017**, *77*, 1327.

[49] D. Baş, İ. H. Boyacı, *J. Food Eng.* **2007**, *78*, 836.

[50] T. F. Edgar, D. M. Himmelblau, L. S. Lasdon, *Optimization of Chemical Processes*, McGraw-Hill, Boston, MA **2001**.

[51] S. Ko, M. N. V. Sastry, C. Lin, C.-F. Yao, *Tetrahedron Lett.* **2005**, *46*, 5771.

[52] A. Khazaei, A. R. Moosavi-Zare, H. Afshar-Hezarkhani, V. Khakyzadeh, *RSC Adv.* **2014**, *4*, 32142.

[53] M. Tajbakhsh, H. Alinezhad, M. Norouzi, S. Baghery, M. Akbari, *J. Mol. Liq.* **2013**, *177*, 44.

[54] M. Tajbakhsh, H. Alinezhad, M. Norouzi, S. Baghery, M. Akbari, *J. Mol. Liq.* **2013**, *177*(Suppl. C), 44.

SUPPORTING INFORMATION

Additional Supporting Information may be found online in the supporting information tab for this article.

How to cite this article: Khazaei A, Mahmoudiani Gilan M, Sarmasti N. Magnetic-based picolinaldehyde–melamine copper complex for the one-pot synthesis of hexahydroquinolines via Hantzsch four-component reactions. *Appl Organometal Chem*. 2017;e4151. https://doi.org/10.1002/aoc.4151